WATER RESOURCES RESEARCH, VOL. 35, NO. 9, PAGES 2671–2683, SEPTEMBER, 1999

Bayesian method for hydrogeological site characterization using borehole and geophysical survey data: Theory and application to the Lawrence Livermore National Laboratory Superfund site

Souheil Ezzedine, Yoram Rubin, and Jinsong Chen

Department of Civil and Environmental Engineering, University of California, Berkeley

Abstract. A stochastic Bayesian approach for combining well logs and geophysical surveys for enhancing subsurface characterization is presented. The main challenge we face is in creating the bridge to link between ambiguously related geophysical surveys and well data. The second challenge is imposed by the disparity between the scale of the geophysical survey and the scale of the well logs. Our approach is intended to integrate and transform the well log data to a form where it can be updated by the geophysical survey, and this tends to be a convoluted process. Our approach starts with generating images of the lithology, conditional to well logs. Each lithology image is then used as the basis for generating a series of shaliness images, conditional to well log data. Shaliness images are converted to resistivity images using a site-specific petrophysical model relating between shaliness, resistivity, and lithology, to create the necessary interface with the cross-well resistivity survey. The lithology and resistivity images are then updated using cross-well electromagnetic resistivity surveys. We explored the limits of the approach through synthetic surveys of different resolutions and error levels, employing the relationships between the geophysical and hydrological attributes, which are weak, nonlinear, or both. The synthetic surveys closely mimic the conditions at the LLNL Superfund site. We show that the proposed stochastic Bayesian approach improves hydrogeological site characterization even when using low-resolution resistivity surveys.

1. Introduction

Combining ground-surface or cross-well geophysical surveys with well logs for enhancing the quality of subsurface characterization has been the goal of recent studies. The primary motivation has been the recognition that geophysical surveys offer unique opportunities for enhancing cross-well interpolation and are particularly promising in situations of data scarcity. *Hyndman et al*. [1994] developed an inversion algorithm that employs both seismic cross-well travel times and solute tracer concentration to estimate the interwell geology and therefore the hydraulic parameters. *Sheets and Hendricks* [1995] used regression techniques to build a site-specific petrophysical relationship between the soil water content estimated from borehole neutron probes and the bulk electrical conductivity of the soil estimated from electromagnetic (EM) induction surveys. This model was then used for mapping the soil water content. *Daily et al*. [1992] conducted an infiltration experiment to build a site-specific regression model between the resistivity and moisture, and showed the potential capability of electrical resistivity tomography (ERT) to monitor capillary barriers performance and flow in the vadose zone. *Doyen* [1988] used cokriging to estimate porosity from surface seismic data and well logs. *Cassiani et al*. [1998] included seismic tomography data and sonic data using a geostatistical approach to improve the estimation of the hydraulic conductivity. *Lucet and Mavko* [1991] combined cross-well seismic tomography, logs, and petrophysical relationships between porosity, velocity, and clay content to estimate porosity and lithology. *Rubin et al*. [1992] and *Copty and Rubin* [1995] used a Bayesian approach and maximum likelihood principles to combine seismic velocity with sparsely measured hydraulic conductivity and pressure for the purpose of mapping the spatial distribution of the hydraulic conductivity. Copty and Rubin showed that integrating geophysical and hydrological data enhances the estimation of the hydraulic conductivity despite the uncertainty and errors associated with the interpretation of the seismic velocity. *Hubbard et al*. [1997] used a similar approach to incorporate the spatial distribution of dielectric constant obtained from ground-penetrating radar (GPR) to estimate soil saturation and permeability in the vadose zone in the case of bimodal spatially-distributed hydraulic conductivity distribution. More recently, *Hubbard et al*. [1999] combined acoustic tomography with borehole data to estimate the spatial covariances of the log conductivity.

A few observations based on these studies are as follows: (1) No universal methods or petrophysical models are available for converting geophysical attributes to hydrogeological ones; (2) The most challenging problem is tying well-logging measurements to the geophysical surveys. This issue involves problems of scale disparity and inconsistencies in the methods of data acquisition and interpretation. The last problem can be demonstrated by the fact that resistivity at the Lawrence Livermore National Laboratory (LLNL) site, which we explore later in this paper, was measured along boreholes using several different tools, each characterized by a different support volume, sometimes leading to dramatically different results.

The present paper investigates the use of geophysical data and surveys for mapping lithology and soil properties in the subsurface using a Bayesian approach [*Copty and Rubin*, 1995].

Paper number 1999WR900131.
0043-1397/99/1999WR900131$09.00

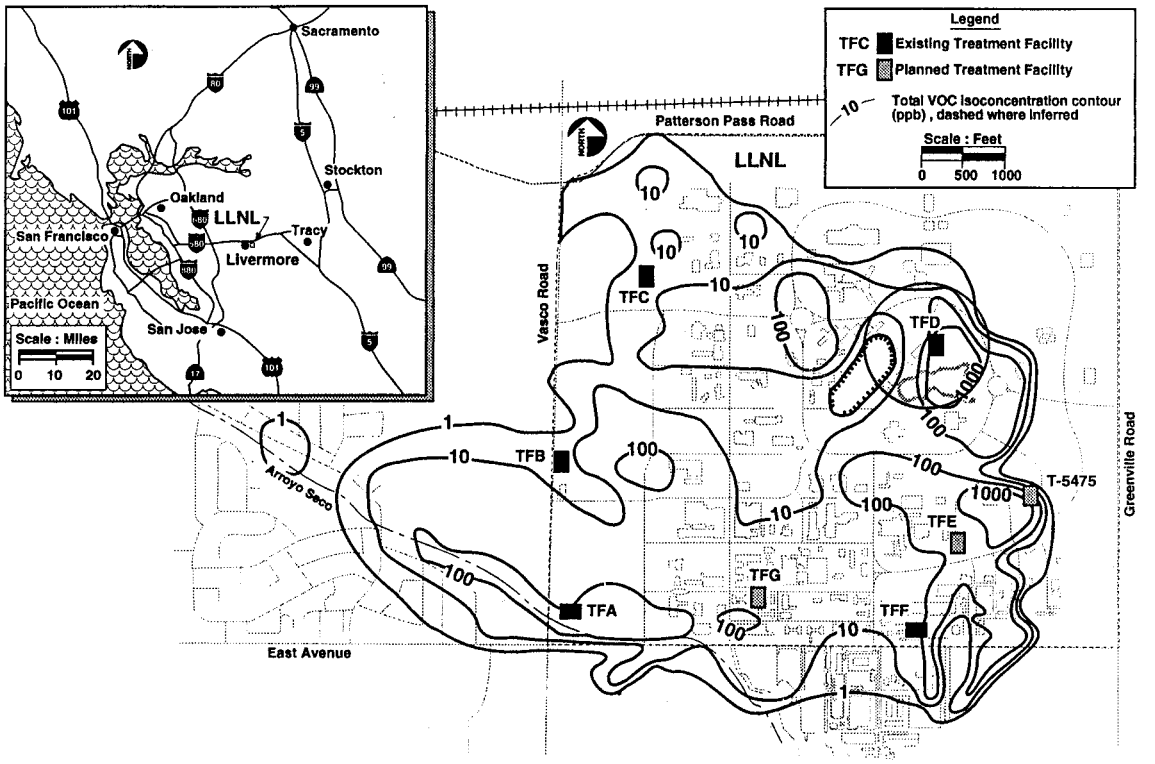

Figure 1. Site map of LLNL showing treatment facility (TF) areas and total volatile organic compounds (VOCs) contoured without respect to depth. Our analysis is focused on the treatment facility D (TFD) shown on the right-hand side. From *Blake et al*. [1995].

The study focuses primarily on the issues and problems associated with the assimilation of weakly or nonlinearly correlated data that are characterized by different spatial resolutions, in a geologically complex environment.

The paper includes five sections. Section 2 introduces the LLNL superfund site and presents a geostatistical analysis of the data. A petrophysical relationship between geophysical and hydrological variables is also presented. Section 3 outlines in detail our approach for data interpretation, principles, and application. Section 4 introduces the synthetic electromagnetic survey, and section 5 discusses Bayesian updating of presimulated lithology and resistivity random fields and evaluates the effectiveness of the proposed approach. Section 6 summarizes all findings.

2. Site Description, Sources of Data, and Geostatistical Analysis

2.1. Lawrence Livermore Superfund Site

Volatile organic compounds (VOC) were used at the LLNL superfund site (Figure 1) as solvents when the site was an active Naval Air Force base in the 1940s. Fuel petroleum hydrocarbons associated with a gasoline spill have also contaminated the underlying aquifer. The VOCs are classified as mainly trichloroethylene (TCE), tetrachloroethylene (PCE), and chloroform. Tritium and chromium are also present, but in smaller concentrations [*Noyes*, 1991]. The site is located in an unconsolidated alluvial basin. The hydrogeology of the area is very complex, but a considerable amount of geological, geophysical, hydraulic, and geochemical data are available. These data provide a unique opportunity to study the relationship between hydraulic conductivity and sediment texture. We focus our analysis on the area near treatment facility D (TFD) shown in Figure 1. The locations of the boreholes which are used in the present analysis are depicted in Figure 2a.

The contaminants are distributed within a thick, complex sequence of unconsolidated alluvial sediments [*Blake et al*., 1995]. A hydrostratigraphic analysis has been conducted to divide this sequence of layers into hydrostratigraphic units (HSUs). These latter are defined as sedimentary sequences whose permeable layers show evidence of hydraulic connectivity, using several complementary sources of information [*Blake et al*., 1995] including chemical (concentration in groundwater and soil), geological (lithological core description), geophysical (wire line borehole electrical logs), and hydrogeological (hydraulic well tests, hydraulic communication between layers). Thicker aquitards were also defined as HSUs, while minor aquitards define HSU boundaries across which little or no vertical hydraulic leakage takes place (Figure 2b).

2.2. Lithological and Geophysical Raw Data

We focus our efforts on the cross section between wells 1206, 1208, 1205, 1252, 1250, and 1251–1254 (Figure 2a), at HSU2, shown in Figure 2b. Spatial statistics are inferred from all available data and wells in HSU2. Types of data collected along the wells include geophysical well log data and lithology. These various data are characterized by different vertical spatial resolution along the boreholes, varying from 3 cm to 15 cm.

Geophysical well log data collected at the site include induction resistivity, short and long normal resistivity, spontaneous potential, single-point resistance, guard resistivity, caliper, and gamma ray, among others. A general description of these log

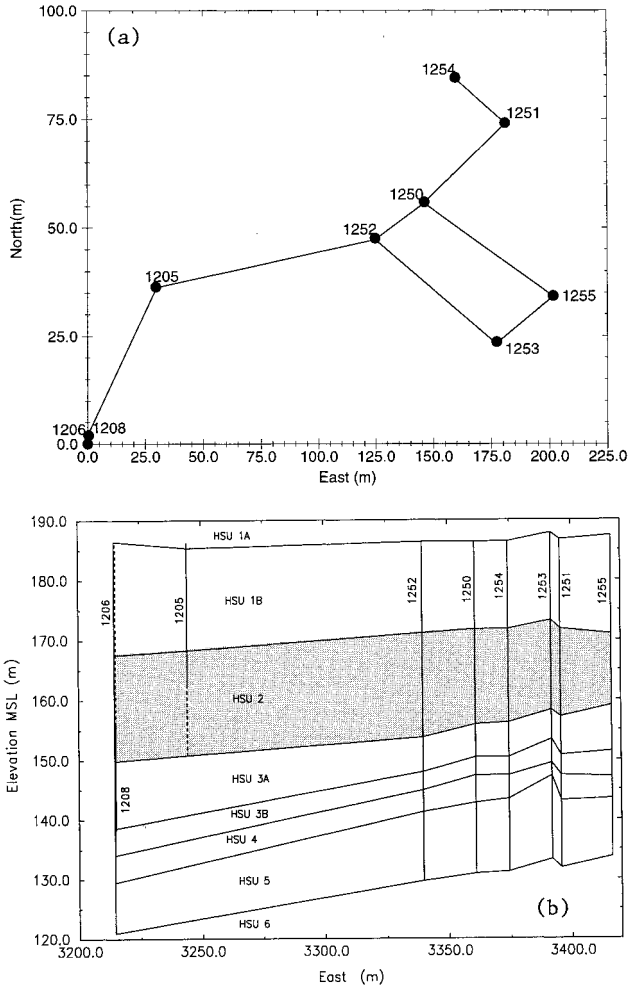

Figure 2. (a) Location of the wells available for the present study in TFD. Nine wells are depicted and labeled 1205, 1206, 1208, and 1250 through 1255. (b) Vertical cross section over all hydrostratigraphic units (HSUs) through all wells depicted on Figure 2a. Vertical dash lines represent missing data. HSUs are referred by their name HSU 1 through 6. Our analysis is focused on the shaded HSU referred to us as HSU2.

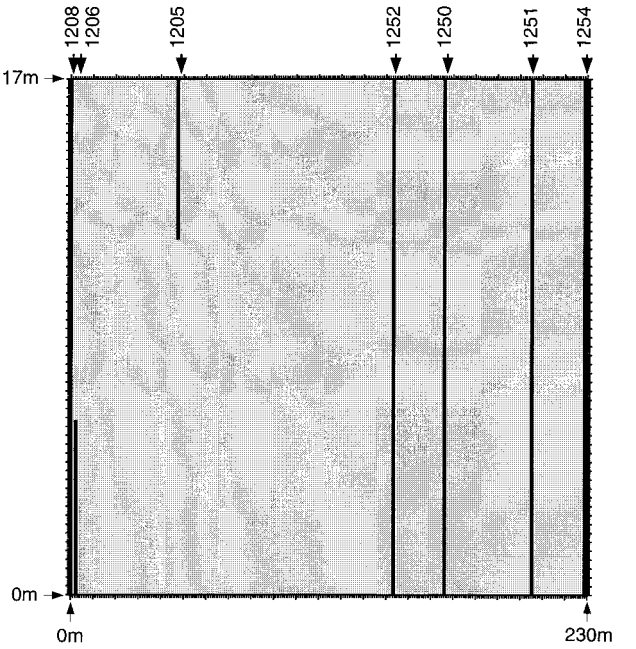

Figure 3. Vertical cross-section of the present study over HSU2 and only through wells 1206, 1208, 1205, 1252, 1250, and 1251–1254. Distances are reported from well 1206 and along the cross section. Only available data along the wells are depicted using continuous vertical lines.

types is given by *Keys* [1997]. Lithology logs were classified as gravel, clay, sand, silt, and mixtures, such as, gravelly clay, clayey sand, totaling 16 different lithologies. To simplify the mapping of the lithologies, and because we are particularly interested in mapping the high and low hydraulic conductivity zones, only two main classes will be used: (1) silt, which includes all silts, clays, and their mixtures, and (2) sand, which includes all sands, gravels, and their mixtures.

2.3. Geostatistical Well Log Analysis

Since the HSUs are not horizontal and are not defined by constant thickness (Figure 2b), the vertical coordinates were normalized by the average thickness of the HSU, which is $\simeq$17 m (Figure 3). An indicator semivariogram was used to characterize the spatial variability of the lithologies on the basis of a binary representation for sand and silt. Semivariograms have also been used to characterize gamma-ray (G) and resistivity (R) spatial variability. Those variables were investigated with and without log transformation. Semivariograms of geophysical attributes within each lithology were also investigated. The reason for presenting the statistics of these three variables is in the fact they form the basis of our method for utilizing the resistivity survey.

2.3.1. Lithology indicator semivariograms. On the basis of the silt/sand classifications and adopting an indicator coding of 0 for sands and 1 for silts, a geostatistical analysis of the lithofacies was performed. Figures 4a and 4b depict the vertical and horizontal indicator semivariograms. Because the vertical semivariogram was computed after normalizing the depth by the thickness of HSU2, the maximum lag is equal to the average thickness of the HSU2. The volume fractions of silts, p, and sands, $(1 - p)$, are 0.48 and 0.52, respectively. The sills of the semivariograms are 0.25, equal to the theoretical value of the variance of the population which is $p(1 - p)$. The theoretical models fitted to the data are exponential with a range of 1.5 m in the vertical direction, and 30 m in the horizontal direction.

2.3.2. Resistivity measurement analysis. The analogies between the flow of electrical current and fluid through porous media have made electric logging of the formation resistivity a commonly employed technique in geophysical prospecting [*Keys*, 1997]. Since a cross-well electromagnetic resistivity survey is considered at the LLNL site, well log resistivities were considered as the primary means for tying and correlating the tomographic survey with other soil properties.

Semivariograms of induction resistivity, guard resistivity and short and long resistivities were investigated; yet well-defined, long-range patterns of spatial correlation were not identifiable. Despite the apparent lack of spatial correlation of the resistivity, we found that the combination of induction resistivity with gamma-ray and lithology logs offers an opportunity for indirect conversion of gamma-ray and lithology pairs into estimates of resistivity. This option will be explored below.

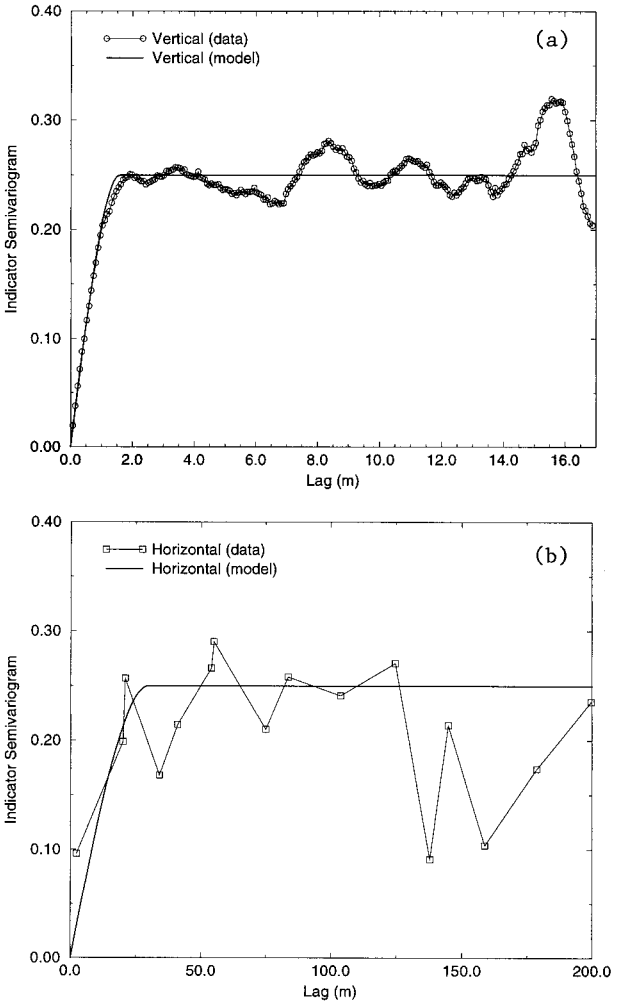

Figure 4. Indicator experimental and theoretical semivariograms: (a) vertical direction and (b) horizontal direction. Both theoretical semivariograms are found to be exponential.

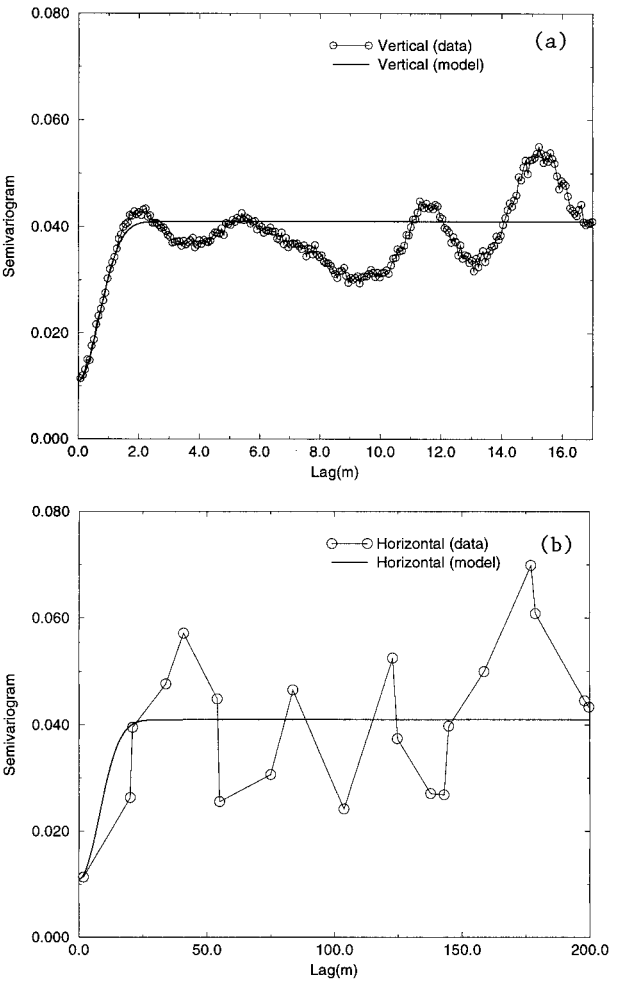

Figure 5. Shaliness experimental and theoretical semivariograms: (a) vertical direction and (b) horizontal direction. Both theoretical semivariograms are found to be Gaussian.

Our choice of induction resistivity among all the resistivity logs as the primary candidate for correlation with the resistivity survey is based on several observations: (1) The measurement procedure does not require conductive fluid in the borehole or direct physical contact with the formation. (2) Induction tools minimize the contribution of the borehole, invaded zone, and surrounding formations on the measurement. (3) Induction logs are automatically corrected for skin effect during recording. (4) Although induction tools were designed for nonconductive borehole environments, they are found to yield excellent measurements in water-based mud, provided that the water is not too salty, the formation is not too resistive, and the borehole diameter is not too large [*Keys*, 1997]. The induction log measurements at the LLNL are of excellent quality, which reinforced our choice.

2.3.3. Gamma-ray analysis. Gamma-ray logs measure naturally occurring gamma emissions around the borehole. The sources of the radioactive decay series in nature are primarily potassium 40, uranium 238 and 235, and thorium 232 [*Serra*, 1986]. Potassium 40 is by far the most abundant radioactive isotope found in sediments. As the content of potassium 40 increases, the response of the gamma-ray probe increases. Gamma-ray response decreases from shales and clays, to siltstone, to sandy siltstones, to sandstones and gravels.

Conversion of gamma-ray measurements to shaliness helps to remove inconsistencies in the data introduced by using different tools and calibration techniques [*Doveton*, 1986; *Hill*, 1986]. Shaliness for unconsolidated rock is given by [*Serra*, 1986]

$$S = 0.083[2^{3.7I_G} - 1] \tag{1}$$

where I_G, the gamma-ray index, is defined as follows [*Serra*, 1986]:

$$I_G = \frac{G - G_{\text{Min}}}{G_{\text{Max}} - G_{\text{Min}}} \tag{2}$$

Figures 5a and 5b depict the vertical and the horizontal semivariograms of the shaliness and the fitted models. The best fit was found to be a Gaussian model with a nugget equal to 0.011 and ranges of 2.5 m in the vertical direction and 25 m in the horizontal direction. Integral scales are set to 1.46 m ($\simeq$1.5 m) and 14.43 m ($\simeq$14.5 m) in the vertical and the horizontal directions.

2.3.4. Shaliness versus resistivity relationship. Figure 6a displays a cross plot of the resistivity and shaliness. Two main

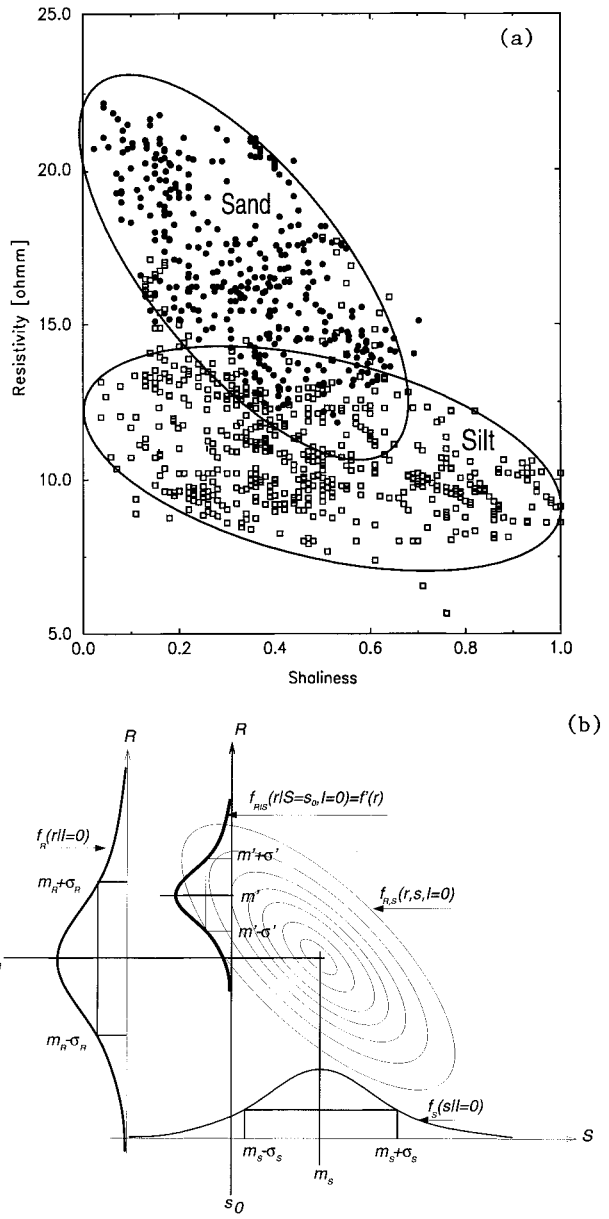

Figure 6. (a) Petrophysical relationship between shaliness and resistivity plotted from available data at the wells crossing HSU2. (b) Generic scheme for constructing resistivity pdfs to conditional lithology and shaliness.

clusters are shown, corresponding to the different lithologies. Figure 6a suggests that resistivity-shaliness pairs are useful for lithology identification. The overlap between the sand and silt clusters indicates that a unique identification of lithology based on resistivity and shaliness is possible for most, though not all, pairs. The main reason for the overlap between the two clusters is data reduction: the original lithology classification consisted of 16 members, which we have reduced to only two. Despite the ambiguous interpretation of several pair combinations, it appears that this cross plot is a good analytical tool. This is one of the fundamental results of our analysis so far, since it suggests a systematic approach for tying the geophysical survey with well logging information. The approach is developed in section 3.

Figure 6a was obtained using all well log data within the HSU2. The use of shaliness instead of gamma-ray activity considerably improved the clustering analysis. This analysis has been applied to other HSUs as well, and in all cases we observed a behavior similar to that shown in Figure 6a.

3. Bayesian Data Assimilation

In an ideal situation the geophysically measured attributes correlate well with the hydrogeological ones, e.g., permeability, and the conversion of the geophysical survey to a hydrogeological distribution map is straightforward. In more realistic situations, such as the one described here, the conversion of the geophysical attributes to the hydrogeological ones is convoluted and nonunique. The difficulties we face in the implementation of the geophysical survey are several. First, we expect the survey resistivity to be of relatively low resolution. At the same time, we need to develop high-resolution permeability images, and hence we face a problem of scale disparity. Additionally, the database available at the site was developed over many years (regardless of our survey!), and hence the types of data highest on our wish list are not available. For example, the cores were not tested for permeability. Hence our study can also be defined as "the art of the possible."

The purpose of this section is to develop a conceptual, data-driven approach for lithology mapping based on the well log data. The proposed approach is general in its basic principles but at the same time is site-specific since the petrophysical models employed are not universal. The general approach is stochastic. The choice is justified given the large uncertainty associated with cross-well interpolation, with the petrophysical models and with the interpretation of the geophysical surveys. The rationale for our approach is based on the following observations:

1. Resistivity and shaliness can be used for lithology identification through the cross plot (Figure 6a). Once a type of lithology is determined, further mapping of hydrogeological properties can be pursued.
2. Facies identification based on the shaliness-resistivity crossplot is nonunique owing to some overlap between the sand and silt clusters.
3. Borehole resistivity measurements display short correlation range, and it is impractical to develop spatial images of the resistivity using cross-well geostatistical interpolation.
4. Shaliness displays a well-defined spatial correlation structure. It can be used for projecting resistivity measurements indirectly through a combination of geostatistical interpolation-simulation techniques, in conjunction with the nonlinear correlation structure it displays with the resistivity, as expressed through the cross plot (Figure 6a).

Based on these observations we propose an approach which consists of sequentially generating a series of collocated attributes. At the basis of the hierarchy, images of the lithology are generated, conditional to well logs and possibly also to the survey resistivity. Each lithology image serves then as the basis for generating a series of shaliness images, again conditional to well data. The shaliness images are then used to correlate the survey resistivity with the hydrogeological attributes obtained experimentally. The series of generated images all have in common the well data and the same underlying spatial structure, and hence they are all physically plausible. The variations between the images constitute a measure of the spatial variability and estimation uncertainty. Our focus here is on estimating resistivity, but it can be converted to porosity and con-

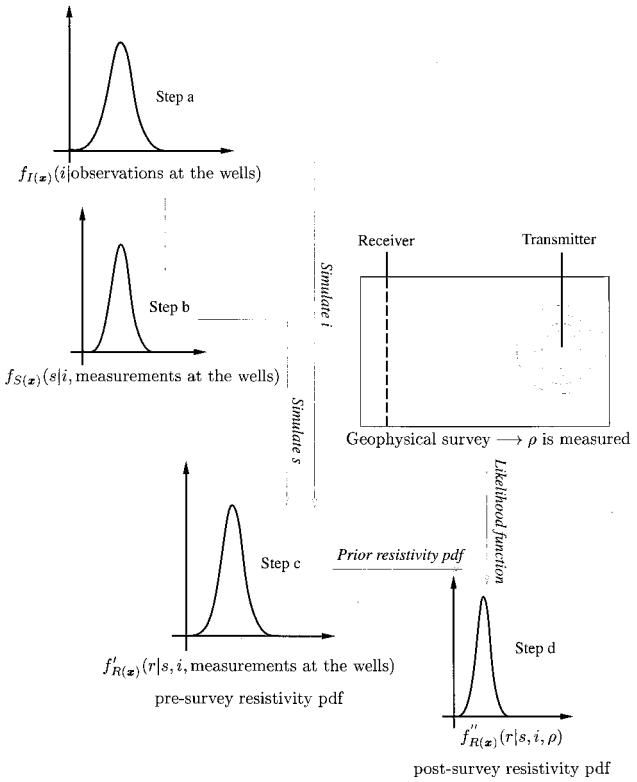

Figure 7. A flow chart for a generic point **x**.

ductivity through well known models such as Archie's, Waxman-Smits', Kozeny-Carmen's [*Mavko et al*., 1998], or through site-specific calibration curves [e.g., *Daily et al*., 1992].

3.1. Outline of the Approach

After the exploratory data analysis is performed as previously described, we proceed in four steps as described below. An accompanying flow chart is shown in Figure 7.

3.1.1. Step 1: Generation of the lithology images using sequential indicator simulation (SIS). The lithology is defined through an indicator variable I according to [*Rubin*, 1995]:

$$I(\mathbf{x}) = \begin{cases} 1 & \mathbf{x} \text{ in silt} \\ 0 & \text{otherwise} \end{cases} \tag{3}$$

Note that boldface letters denote vectors; i.e., **x** is the location coordinates vector. Lowercase i is a realization of the spatial random function (SRF) I. I is characterized through its unconditional expected value, which is assumed stationary:

$$E\{I\} = p \tag{4}$$

where E denotes the expected value operator and p is the volume fraction of silts. Its pattern of spatial variability is defined through the semivariogram

$$\gamma_I(\mathbf{x}, \mathbf{x}') = \tfrac{1}{2}E\{(I(\mathbf{x}) - p)(I(\mathbf{x}') - p)\} \tag{5}$$

and is shown in Figure 4.

The unconditional statistics define the crudest level of probabilistic characterization. A more advanced characterization is possible through the conditional moments of I. These statistics are the cornerstone of the SIS algorithm [*Deutsch and Journel*, 1998; *Rubin and Bellin*, 1998] which we adopt here. The SIS algorithm consists of computing the expected value of I conditional to the borehole data:

$$p^{\mathrm{c}} = E^{\mathrm{c}}\{I\} = E\{I|\{\text{measurements}\}\} \tag{6}$$

with a superscript c denoting conditional.

Since I is binary, p^{c} is statistically exhaustive. Hence once p^{c} is defined, a realization of I can be drawn, with p^{c} as the target statistic. The process of computing p^{c} and drawing realizations is done sequentially over a grid. Spatial continuity is maintained by conditioning I not only on well data but also on all the previously generated values. Specifically,

$$p^{\mathrm{c}} = p + \sum_{n=1}^{N} \lambda_n (I(\mathbf{x}_n) - p) \tag{7}$$

where the weights λ_n are obtained by solving the following system of linear equations:

$$\sum_{n=1}^{N} \lambda_n \gamma_I(\mathbf{x}_m, \mathbf{x}_n) = \gamma_I(\mathbf{x}_m, \mathbf{x}), \quad m = 1, \cdots, N \tag{8}$$

The important point to note is that N, the number of lithology measurements, includes all the observations as well as the values generated at all the nodes other than **x**.

3.1.2. Step 2: Generation of shaliness images. This step is similar in principle to the previous one. The differences are in the fact that (1) the shaliness S is not a binary variable and (2) the pattern of spatial variability of the shaliness may be different between the sand and silt lithologies; i.e., $\gamma_{S|i}$, the semivariogram of the shaliness S, depends on the lithology $i = 0$ or 1:

$$\gamma_{S|i}(\mathbf{x}, \mathbf{x}') = \tfrac{1}{2}E\{(S(\mathbf{x}|i) - m_{S|i})(S(\mathbf{x}'|i) - m_{S|i})\} \tag{9}$$

The univariate and spatial statistics of the shaliness were discussed in section 2. Hence at this step we compute, using the kriging equation, the conditional mean and variance of S, which define the target statistics. Subsequently, using a Gaussian random generator, a local value for S is drawn from the distribution. Defining the shaliness S through its mean $m_{S|i}$ and its semivariogram $\gamma_{S|i}$ for a given lithology i, the conditional mean $m^{\mathrm{c}}_{S|i}$ and variance $\sigma^{2\mathrm{c}}_{S|i}$ of the shaliness are given by

$$m^{\mathrm{c}}_{S|i} = \sum_{l=1}^{N} \alpha_l S(\mathbf{x}_l|i) \tag{10}$$

$$\sigma^{2\mathrm{c}}_{S|i} = \sigma^2_{S|i} - \sum_{l=1}^{N} \alpha_l \operatorname{Cov}_{S|i}(\mathbf{x}_l, \mathbf{x}) \tag{11}$$

where the covariance is identified by $\operatorname{Cov}_{S|i}(\mathbf{x}_l, \mathbf{x}) = \sigma^2_{S|i} - \gamma_{S|i}(\mathbf{x}_l, \mathbf{x})$, and the weights α_l are obtained by solving the following system of linear equations:

$$\sum_{l=1}^{N} \alpha_l \operatorname{Cov}_{S|i}(\mathbf{x}_m, \mathbf{x}_l) = \operatorname{Cov}_{S|i}(\mathbf{x}_m, \mathbf{x}), \quad m = 1, \cdots, N \tag{12}$$

All points l, $m = 1, \cdots, N$ are located within the lithology i.

3.1.3. Step 3: Computing the resistivity prior probability density function. Once **x** is identified as being either sand or silt and is assigned a shaliness value, a prior probability density

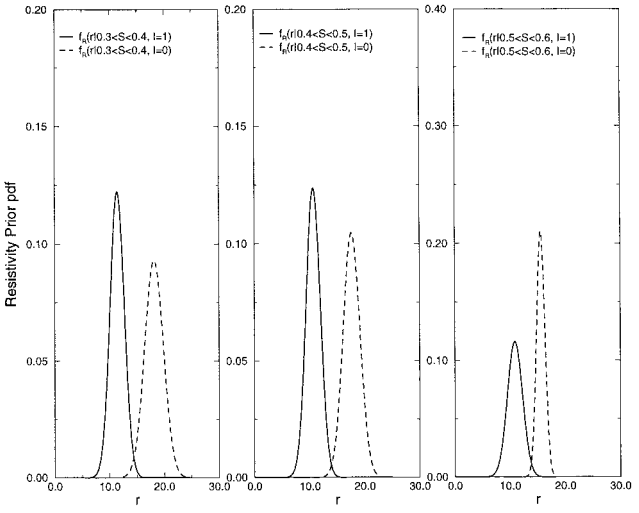

Figure 8. Examples of prior pdf's $f'(r)$ for $I = i$, $i = 0, 1$ and shaliness $0.3 < s < 0.6$.

function (pdf) for the resistivity $f_{R(\mathbf{x})}(r|I = i, S = s)$ can be defined through Figure 6a. R and S denote the space random function (SRF) of the resistivity and the shaliness, respectively, and r and s denote their realizations. Figure 6b illustrates the joint pdf of R and S given $I = 0$ (i.e., sand lithology) and the marginals $f_R(r|I = 0)$ and $f_S(s|I = 0)$. Conditioning further on $S = s_0$ leads to $f_{R|S}(r|S = s_0, I = 0)$, which is our Bayesian prior. Scarcity of data led us to condition on ranges of S values rather than on single values. Examples of $f_{R(\mathbf{x})}(r|I = i, 0.3 \le s \le 0.4)$, $f_{R(\mathbf{x})}(r|I = i, 0.4 \le s \le 0.5)$, and $f_{R(\mathbf{x})}(r|I = i, 0.5 \le s \le 0.6)$ for $i = 0, 1$ are shown in Figure 8. These pdfs are the Bayesian prior pdfs of the resistivity, and hence our stochastic estimation for the resistivity R at $\mathbf{x}$ in case no additional data become available through surveying.

3.1.4. Step 4: Updating $f_{R(\mathbf{x})}(r|I = i, S = s)$ on the basis of cross-well electromagnetic resistivity survey $\rho(\mathbf{x})$. Defining $f_{R(\mathbf{x})}(r|I = i, S = s) = f'_{R(\mathbf{x})}(r)$ for brevity, and given a collocated survey resistivity $\rho(\mathbf{x})$, the posterior pdf $f''_{R(\mathbf{x})}(r|\rho)$ can be defined through Bayes' rule [*Ang and Tang*, 1975]:

$$f''_{R(\mathbf{x})}(r|\rho) = C_R L(\rho|r) f'_{R(\mathbf{x})}(r) \tag{13}$$

where $L(\rho|r)$ is the likelihood function and C_R is a normalized factor defined as [*Ang and Tang*, 1975]

$$C_R = \left(\int_{-\infty}^{\infty} L(\rho|r) f'_{R(\mathbf{x})}(r)\, dr \right)^{-1} \tag{14}$$

In general, ρ is defined over a support volume larger than the support volume of r. Note that in the case of a high-resolution geophysical survey, $\rho(\mathbf{x}) \to r(\mathbf{x})$, and Bayesian updating is unnecessary. In this case, ρ can simply be converted to the hydrogeological properties of interest if a petrophysical model is available. That conversion will be as reliable and accurate as the petrophysical model used for conversion. This, however, is not generally the case, and the alternative is to update $f'_{R(\mathbf{x})}(r)$ given ρ. Typically, we are interested in R representative of a block of scale ~1 m while ρ is defined by blocks of scale ~3 m or greater. The inference of the likelihood function, $L(\rho|r)$, is critical for the successes of the update and is discussed in section 5. Once $f''_R(r|\rho)$ is defined, however, a realization of R at $\mathbf{x}$ can be drawn. The whole process is repeated for all $\mathbf{x}$ until a complete image of the resistivity field is completed.

An attractive property of Bayesian updating is that the posterior $f''_{R(\mathbf{x})}(r)$ is at least as informative as $f'_{R(\mathbf{x})}(r)$. In the case of a totally noninformative likelihood function, $L(\rho|r)$ equals $L(\rho)$, and equation (13) yields $f'_{R(\mathbf{x})}(r) = f''_{R(\mathbf{x})}(r)$. It is emphasized that the method does not always guarantee better estimates for a couple of reasons. First, the Bayesian approach provides a pdf, not a single valued estimate. Second, the improvement achieved in the posterior pdf is dictated by the quality of external factors such as the accuracy of the geophysical survey and the petrophysical model.

A modification of step 1 is appropriate and useful if the lithology images can also be conditioned on the resistivity. As is apparent from Figure 6a, the lithology images can be improved through the resistivity survey: sands tend to be characterized by high resistivities and silts are characterized by low resistivity, although there is some overlap at midrange values. Our approach calls for Bayesian updating of p^c as well, through the relationship

$$p^{c'} = C_I L(\rho|I) p^c \tag{15}$$

where $L(\rho|I)$ is the likelihood function, similar in nature to (14), only relating ρ to I rather than R. C_I is a normalized factor similar to C_R in (14).

3.2. The Synthetic "True" Data Base

The concept outlined in section 3.1 is demonstrated here using a synthetic example, generated to simulate closely the conditions of HSU2. Figure 9a depicts a realization of HSU2 lithology conditional to the lithology observed at the wells. The field is 230 m in the horizontal direction and 17 m in the vertical direction. Realizations of the shaliness and resistivity fields, based on sections 3.1.2. and 3.1.3., conditional to borehole data, are depicted in Figures 9b and 9c. The spatial statistics used are those described in section 2.

4. Electromagnetic Surveying

Field EM surveying is a complex mapping of the detailed, high-resolution $R(\mathbf{x})$ distribution into a low-resolution $\rho(\mathbf{x})$ field. In reality, the geophysical response is distorted by both data acquisition and the inversion process.

An electromagnetic survey was conducted at LLNL through polyvinyl chloride (PVC) cased wells. Two surface to borehole profiles were measured with a surface transmitter loop (frequency 11.3 kHz) and a vertical magnetic coil receiver placed in well 1250. The profiles were in the region between wells 1250–1251 and 1250–1252 shown in Figure 2. Seven cross-well EM data sets were collected. A vertical magnetic coil transmitter (frequency of 9.6 kHz) was placed in well 1250 and 1251. From well 1250, five data sets were collected with a vertical magnetic receiver placed successively in wells 1251 through 1255. The last two data sets were collected between wells 1251–1253 and wells 1251–1254. All data sets from the cross-well EM survey have been processed, but final results are not yet available. To explore the Bayesian updating approach, synthetic surveys of the resistivity are simulated.

The theoretical foundation of the EM survey is based on Maxwell's wave propagation equations. These equations couple the electric field to the magnetic one and are given in Appendix A. Under reasonable approximation of low variability of the resistivity between the sand and the silt bodies (see

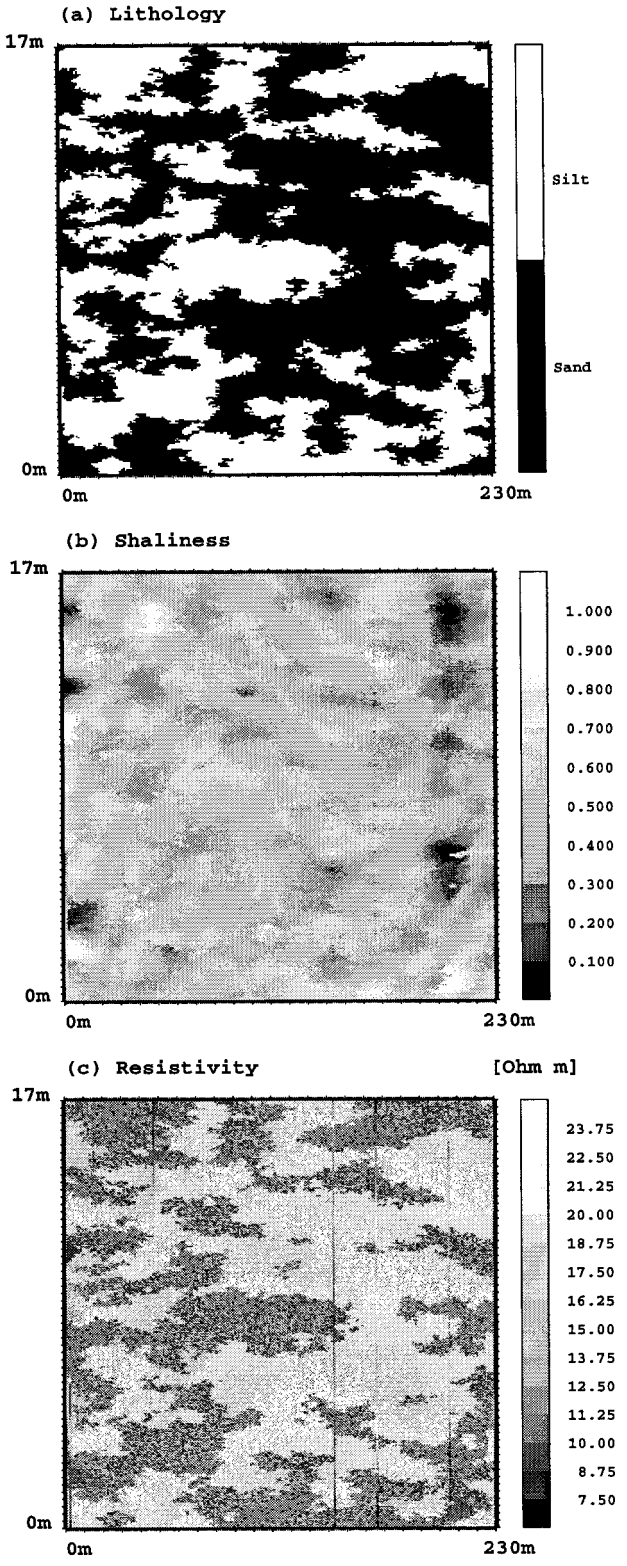

Figure 9. "True" geological setting. (a) Sequential indicator simulation of the lithology conditional to borehole data. Black and white represent sand and silt, respectively. (b) Sequential Gaussian simulation of the shaliness conditional to borehole shaliness measurements. Darker shades represent sand (low clay content), and brighter shades represent silt (high clay content). (c) True resistivity random field built by projecting the "true" shaliness field using the petrophysical relationship depicted in Figure 6a.

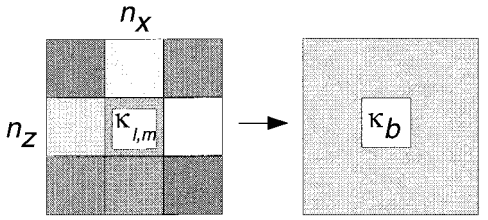

Figure 10. Upscaling small-scale block conductivities $\kappa_{l,m}$, $l = 1, \cdots, n_x$; $m = 1, \cdots, n_z$ into survey scale block conductivity κ_b.

Figure 6a), the wave propagation problem can be reduced to an electric current diffusion problem. Identical problems have been considered in fluid flow in porous media [*Dagan*, 1989] and flow of electric currents [*Abramovich and Indelman*, 1995]. Borrowing from their results, and considering the two-dimensional (2-D) survey, the electrical conductivity κ_b of a block which covers n_x by n_z small-scale blocks (Figure 10), where n_x is the number of blocks in x direction and n_z in the z direction, is given by the geometric mean:

$$\kappa_b = \left(\prod_{l,m=1}^{n_x \times n_z} \kappa_{l,m} \right)^{1/(n_x \times n_z)} \tag{16}$$

where $\kappa_{l,m}$ are the small-scale blocks. This formula is applicable for blocks that are large relative to the characteristic length scale of resistivity heterogeneity. In the present case, since the characteristic length of the spatial variability is small, geometric averaging appears to be the appropriate homogenization procedure.

From simple algebra, $\rho = (\Pi_{l,m=1}^{n_x \times n_z} R_{l,m})^{1/(n_x \times n_z)}$ (see Appendix A). Hence for the purpose of this study, the resistivity of a block detected in a survey equals the geometric averaging of the small-scale resistivities. We shall consider $n_x = n_z = 3$, 6, 9. Figures 11a and 11b show results of synthetically surveying the resistivity field shown in Figure 9c using different resolutions. As the resolution decreases, small-scale details become obscure and fuzzy, and the range of resistivity values detected narrows.

5. Synthetic Case Study

In our case study we investigate the cross-section shown in Figure 3, assuming that Figures 9a to 9c, which were generated conditional to the borehole data, are the "true" images of that cross section. A geophysical survey of the same cross section is simulated using equation (16). Our goal is to test the capability of the method described in section 3 to reconstruct the base case's images while benefiting from the resistivity survey.

Typical images obtained through the use of prior pdf's only are depicted in Figures 12a to 12c. It is noted that these images are in good agreement with the corresponding images (Figures 9a to 9c) but only in the well-sampled areas, on the right-hand side of the images. Figures 12a and 12c will be updated following the methods outlined in sections 3.1.3 and 3.1.4. Updated images will be compared with to the assumed "true" images depicted in Figures 9a and 9c.

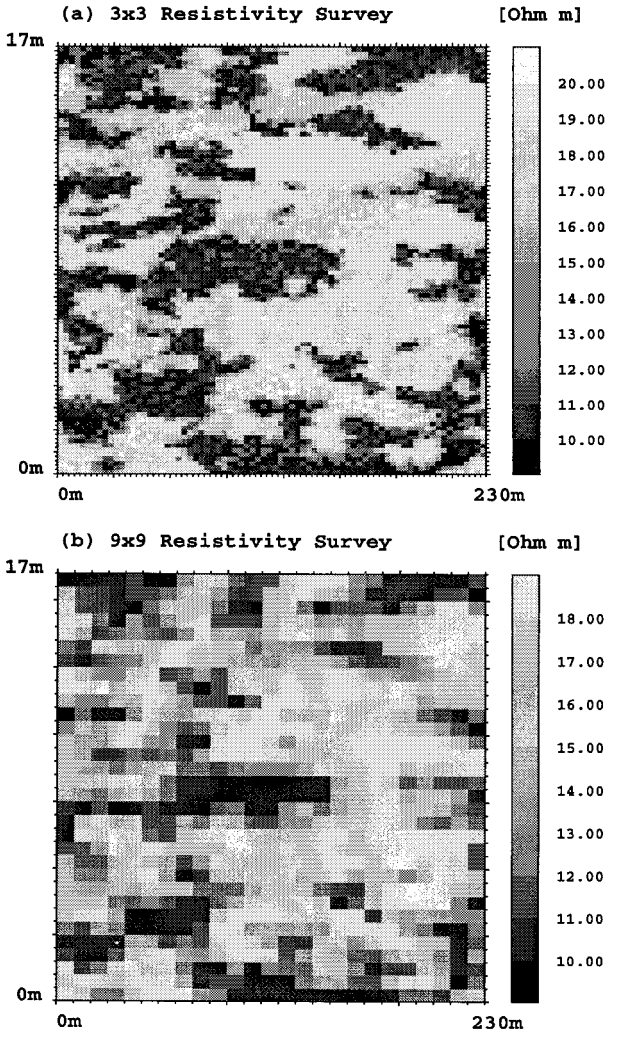

Figure 11. Examples of the resistivity surveys obtained by geometric averaging of the "true" resistivity field (Figure 9c) over (a) three and (b) nine small-scale blocks in the horizontal and vertical directions.

5.1. Indicator Likelihood Functions and Updating the Lithology Images

Equation (15) requires to infer the likelihood function $L(\rho|I)$. To identify L, we use a "training set." The idea is to identify a portion of the survey area that will be drilled and cored post survey to yield a set of collocated measurements (ρ, i). The dimension of the training set area should be determined such that the survey represents the entire range of conditions expected over the entire surveyed area. The sampled area needs to be ergodic in terms of bivariate (ρ, i) statistics. That usually implies a dimension of several integral scales vertically, along cored wells. Values of ρ measured close to the wells can also be considered as located at the well itself. An alternative that is not pursued here is to derive the likelihood function analytically, on the basis of upscaling rules [i.e., *Copty and Rubin*, 1995; *Rubin et al.*, 1992]. In the present application the well-sampled area near well 1250 (right-hand side of Figure 3) was set to be the training set, and the much less sampled area near well 1205 (left-hand side of Figure 3) was set as the "testing set."

$L(\rho|I)$ is determined for a given $I = i$ and $\rho = \rho_0$ by

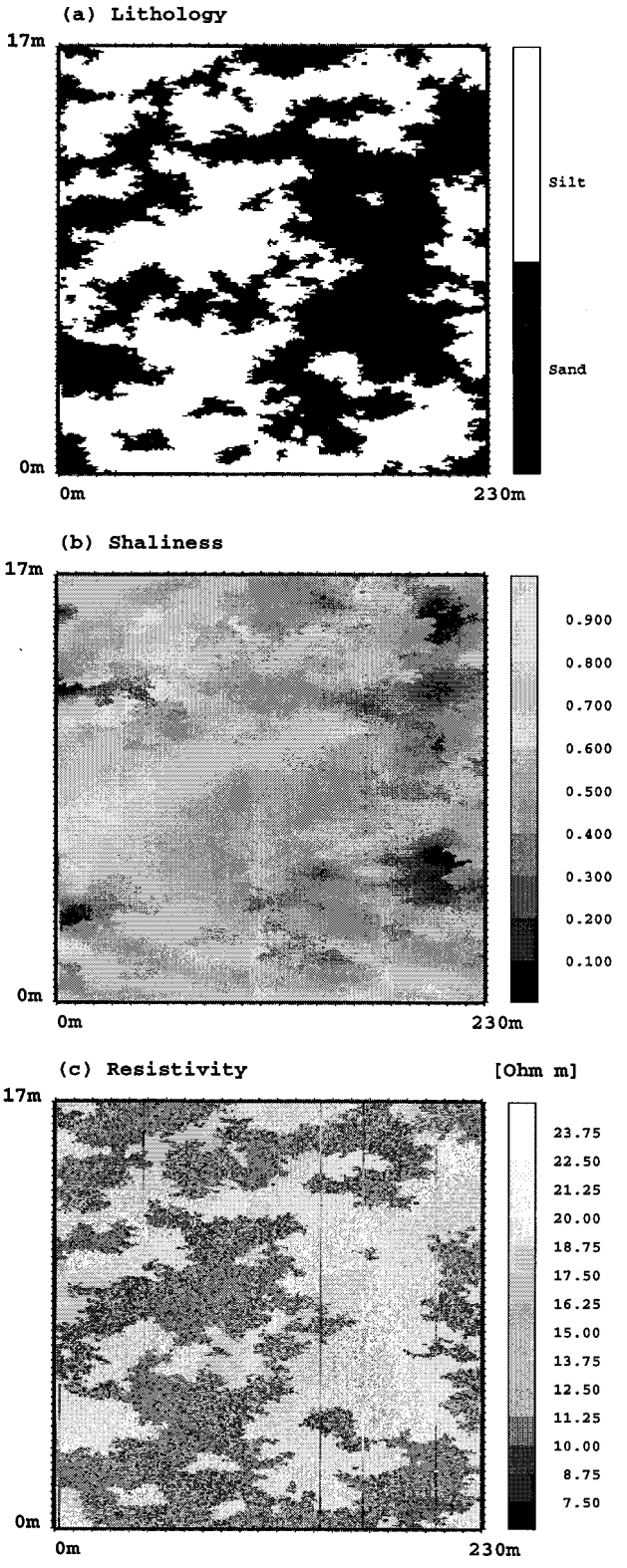

Figure 12. (a) Single realization of the lithology field obtained by sequential indicator simulation of the lithology conditional to borehole core data. Black and white represent sand and silt, respectively. (b) Single realization of the shaliness field obtained by sequential Gaussian simulation of the shaliness conditional to borehole shaliness measurements. (c) Single realization of the resistivity field built by projecting the shaliness random field (Figure 12b) using the petrophysical relationship (Figure 6a).

Figure 13. Posterior lithology image of the "testing set" (left-hand side of Figure 12a, using (15)) and 3×3 resistivity survey (Figure 11a).

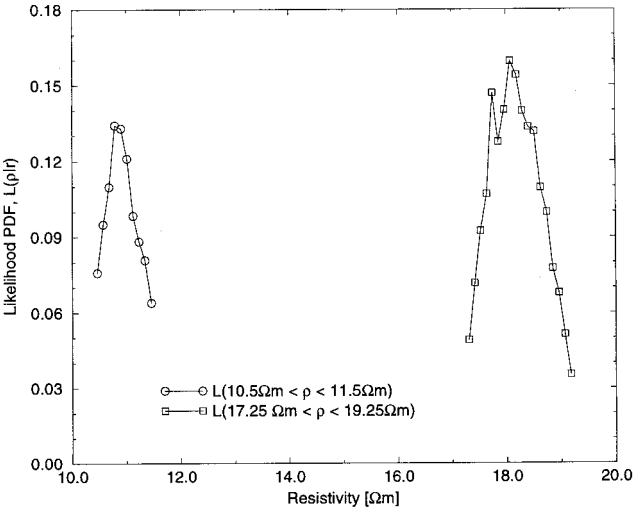

Figure 14. Examples of the likelihood function $L(\rho|r)$ inferred from 3×3 resistivity survey following (13).

scanning the set of collocated pairs (i, ρ_0) and computing the conditional probability Prob$[\rho = \rho_0|I = i]$. Equation (15) is then used to update the lithology image (Figure 12a) using different resistivity survey resolutions. Images of the "testing set" obtained on the basis of (15) for $n_x \times n_z = 3 \times 3$, 6×6 and 9×9 resistivity surveys are practically of the same quality as without updating and differ only by a fraction less than 1% from the prior lithology (Figure 12a), even in case of high-resolution resistivity survey (3×3), Figure 13. This outcome is a manifestation of the effect of the homogenization, which obscures the resistivity-lithology relationship. A large number of resistivity combinations can lead to the same ρ and hence to nonunique relationship between ρ and the lithology.

5.2. Resistivity Likelihood Functions and Updating the Resistivity Images

$L(\rho|r)$ of equation (13) is approximated here by $L(\rho|r - dr \leq \rho < r + dr)$ with a relatively small dr, due to the data scarcity. A couple of typical examples are shown in Figure 14. It depicts likelihood functions for two ranges of resistivity, [10.5, 11.5] Ω m and [17.25, 19.25] Ω m.

The effect of updating the resistivity based on surveys with different resolutions is demonstrated in Figure 15. It shows the prior and posterior resistivity pdf's at arbitrary points within the silt and sand lithologies for various resolutions of the resistivity survey. The maximum beneficial effect is obtained, not surprisingly, through the high-resolution survey, but the positive impact of conditioning R on ρ is discernible even at the low-resolution surveys. The trend of reduction in impact with poorer resolution is evident and is an outcome of the diffuse and noninformative nature of the likelihood function as the discrepancy between the survey scale and the desired resolution scale increases.

Note that conditioning R on ρ does not imply that the randomly generated values will average exactly to yield ρ unless special measures are taken. To honor precisely the surveyed value ρ, a constraint on the generated value is introduced so that the generated r values over any volume corresponding to ρ will average exactly to yield ρ. The procedure is outlined in Appendix B.

Figures 16a and 16b depict the updated resistivity fields for $n_x \times n_z = 3 \times 3$ and 9×9 resistivity survey. These figures should be compared with the "true" image (Figure 9c, left part), and with the image based on the prior pdf's (Figure 11c). It is quite obvious that the resistivity surveys have a significant positive impact, particularly at the high resolution.

5.3. Effectiveness of the Bayesian Updating

To evaluate the effectiveness of the updating procedure, we analyze the following statistic:

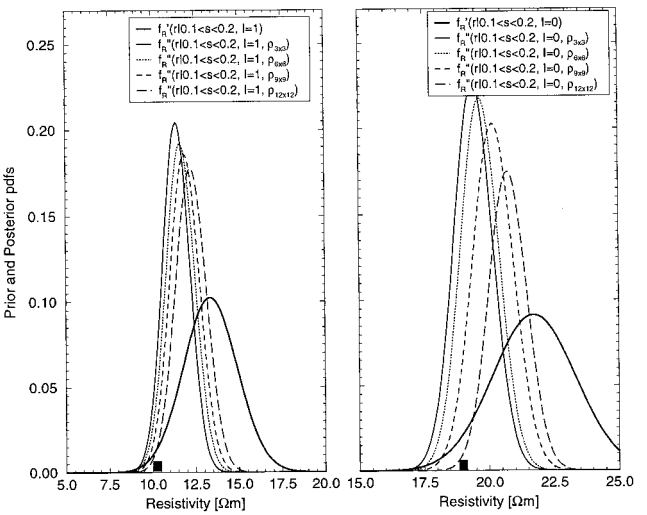

Figure 15. Effect of the resolution of the $n_x \times n_z$ resistivity survey on the posterior pdf's (prior pdf's are also plotted). The bias in the variance and the mean decrease with the increase of the resolution of the resistivity survey (from 12×12, 9×9, 6×6, to 3×3). The black box denotes "true" resistivity values. Prior and posterior pdf's for shaliness between 0.1 and 0.2 in (left) silt ($I = 1$), and (right) sand ($I = 0$).

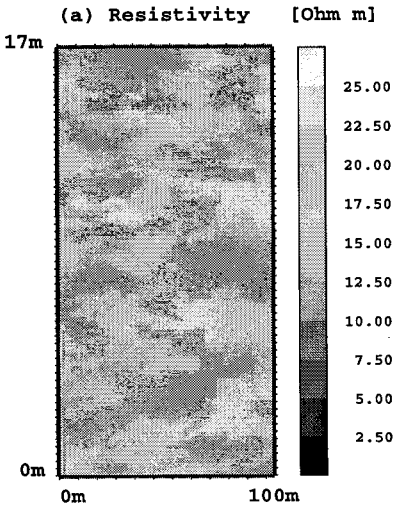

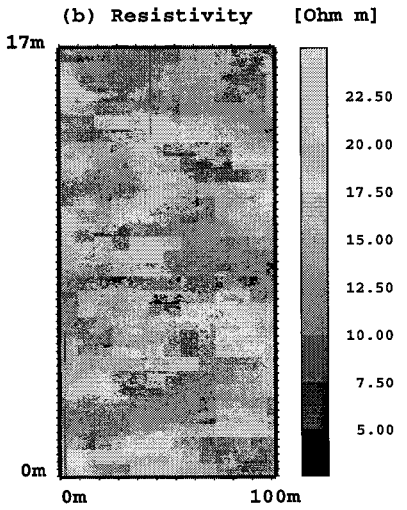

Figure 16. Posterior resistivity images of the testing set (left side of Figure 12c, using (13)) and the resistivity surveys: (a) 3×3 resistivity survey (Figure 11a) and the posterior lithology (Figure 13), and (b) 9×9 resistivity survey (Figure 11c) and the posterior lithology (Figure 13).

$$\mathcal{R}_k = \frac{|r_k - m''|}{|r_k - m'|} \qquad \begin{cases} \mathcal{R}_k < 1 & \text{successful updating} \\ \mathcal{R}_k = 1 & \text{unsuccessful.} \end{cases} \tag{17}$$

where k is a running index over all the points outside the wells, r is the actual resistivity (Figure 9c), m'' is the mean of the posterior pdf $f''_{R(\mathbf{x})}(\mathbf{x})$, and m' is the mean of the prior pdf $f'_{R(\mathbf{x})}(\mathbf{x})$. The ratio $\mathcal{R}$ compares the performance of the posterior and the prior pdfs. $\mathcal{R} < 1$ indicates a successful updating procedure. $\mathcal{R} = 1$ is a diffuse likelihood and hence a noninformative survey. Figure 17 depicts the variation of $\mathcal{R}$, as a function of the resolution of the survey. For completeness, statistics were also computed for resistivity surveys of 2×2 and 12×12 block resolution. We have found that $\mathcal{R}$ decreases with decrease in resolution, in line with Figure 15.

6. Summary

In this study we surveyed some of the problems associated with combining resistivity tomography and resistivity well logging. The focus on resistivity rather than on hydrogeological properties stems from the observation that properties such as permeability and porosity can be derived from the resistivity based on well-documented models or using empirical, site-specific models. We chose to conduct our study by considering conditions as realistic as possible for that purpose. We analyzed the data collected at the LLNL site and synthetically surveyed a cross section that was constructed to mimic closely the geology of the site.

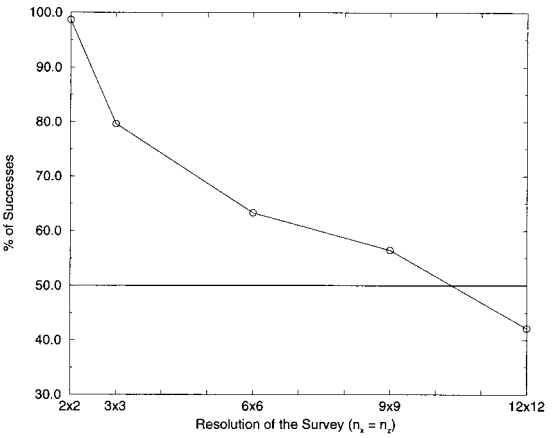

Figure 17. Percentage of number of successes (equation (17)) of the Bayesian updating approach for different survey resolutions and different errors in the surveys.

Our approach for data assimilation is stochastic Bayesian. We find the justification for it in the large spatial variability and data scarcity. The Bayesian approach allows us to condition estimates on what is clearly a set of complex and nonlinear petrophysical models relating between different geological attributes.

The approach we presented here comprises several steps, each of which is intended to explore, model, and utilize the aspects of the data which are needed for relating between the tomographic data and the well logs. However, we stop short of stating that the approach is universal in all its components. The complexity of the geophysical surveying and interpretation makes several aspects of it site-specific.

Our study employed several relationships between induction resistivity, lithology, shaliness and tomographic resistivity. These relationships reflect, to a large degree, properties that are well understood and are quite general in terms of trends. We suspect, though, that these relationships cannot be transported to other sites. In this sense our method does not replace or alleviate the tedious task of data exploration. We found helpful in guiding us at the data exploration stage the need to identify "common-factors": the attributes or parameters that can be used for projecting areally the well log data on the one hand, and at the same time act as surrogates for hydrogeological and geophysical properties. At the LLNL site, that key element is the shaliness, owing to its well-defined spatial structure and its sensitivity to resistivity. The idea then is to employ this variable for projecting well data and generating a prior pdf that is both relevant for the application and that can benefit from the geophysical survey.

Our approach becomes systematic once the "common factors" are identified. At this stage the Bayesian approach becomes the key for data assimilation. Its robustness stems from its ability to express vague relationship as probabilistic rules

and to bridge over scale disparity issues. This brings us to refer to the approach presented here as a set of tools rather than as a clear road map.

Moving now to the more technical aspects of the approach, there are clearly elements that can be changed and/or improved, and there a few issues we would like to mention here. The pdf's in our application all follow Gaussian models. One can argue that pdf's should be accurate reflections of data and not models or conjectures. This issue is particularly significant for the tails of the pdf's. However, our modeling decision here does not impinge on the fundamentals of the approach, which by no means require Gaussian pdf's. We would like to reference here the work of *Woodbury and Ulrych* [1993], who established clear guidelines for choosing priors. These guidelines can be incorporated into our work easily.

Another issue concerns the development of the petrophysical models. Our search leading to Figure 6a was based on visual inspection. However, we can clearly see a need to implement a more systematic approach, especially given that the relationship can be more complex in terms of the number of clusters and the number of the parameters involved.

We would like to bring forward the issue of probability versus similarity. Let us consider Figure 6a. It is obvious that a frequentist interpretation is appropriate over some regions of the cross plot. However, we propose that Figure 6a is somehow a reductionist view of the geology. In fact, the data used in the cross plot do not follow precisely the "either sand or silt" pattern. There are logs that have some similarity to both silt and sand, and may belong to both groups if we allow some flexibility in the degree of membership. That flexibility is not currently a part or our approach: a probabilistic approach can handle and/or situations but not similarity issues. We see a promise in the theory of fuzzy sets [*Bilal and Gupta*, 1997].

Under the conditions explored here, we found that even in the presence of realistic error levels in the geophysical surveys, a significant reduction of the estimation error was observed. We have found that the benefits in estimating high-resolution subsurface resistivity given a low-resolution resistivity survey are more significant than those gained in estimating lithology. The LLNL data showed good correlation between resistivity and lithology at the small scale, but at lower resolution the correlations deteriorate. This observation is supported by the fact that the resistivity surveys were noninformative for updating the lithology images. Resistivity-shaliness-lithology relations may show perfect correlation at a fine scale but can appear to have large scatter when using a larger observation scale.

Finally, a conceptual difficulty we encountered when presenting this approach is the scale discrepancy between the measured ρ and the simulated r. It is emphasized that the scale of r is arbitrary and can be as small as the correlation between ρ and r will support; r is simulated, not estimated.

Appendix A: Synthetic Electromagnetic Survey

The theoretical foundation of the EM survey is based on Maxwell's wave propagation equations. These latter couple the electric field **E** to the magnetic field **H** as follows:

$$\nabla \times \mathbf{E}(\mathbf{x}, t) = -\frac{\partial}{\partial t}\mathbf{B}(\mathbf{x}, t) \tag{A1}$$

$$\nabla \times \mathbf{H}(\mathbf{x}, t) = \frac{\partial}{\partial t}\mathbf{D}(\mathbf{x}, t) + \mathbf{J}(\mathbf{x}, t) \tag{A2}$$

$$\nabla \cdot \mathbf{B}(\mathbf{x}, t) = 0 \qquad \nabla \cdot \mathbf{D}(\mathbf{x}, t) = Q(\mathbf{x}, t) \tag{A3}$$

where **D** is the electric flux, **B** the magnetic flux, **J** is the current density, and Q is the charge density [*Chew*, 1990]. For time varying EM fields, equations (A3) can be derived from the first two equations using the continuity equation given by

$$\nabla \mathbf{J} = -\frac{\partial Q}{\partial t} = -\frac{\partial}{\partial t}(\nabla \cdot \mathbf{D}) \tag{A4}$$

In this static case, the electric field and the magnetic one are decoupled, and the electric field equations can be solved independently from the magnetic ones. This approximation should be viewed as an approximation, applicable in cases where the spatial variability of the conductivity is weak. This approximation has already been used in previous studies [e.g., *Beard et al*., 1996].

In the case of the HSU2 at the LLNL, the mean of the resistivity is 11 Ω m and 17 Ω m, in silt and sand, respectively. The variance of the resistivity in silt and sand are 2 and 3.5 $(\Omega\ \mathrm{m})^2$. These statistics show that the contrasting of variability between and within each silt and sand bodies are similar, and assumptions similar to those of *Beard et al*. [1996] can be made.

Defining the current density **J** as [*Telford et al*., 1990]

$$\mathbf{J} = R^{-1}\mathbf{E};\ \mathbf{E} = -\nabla V \tag{A5}$$

where V is the potential, it satisfies the continuity equation (A4), which leads to

$$\nabla(\kappa \nabla V) = 0 \tag{A6}$$

where $\kappa = 1/R$ is the electric conductivity.

Equation (A6) describes the response of the domain at the smallest scale over which κ can be defined. In a geophysical survey, the small-scale variability cannot be detected. Instead, large parts of the domain are homogenized, and respond as a homogeneous block. The geophysical survey defines the block conductivity, $\kappa_b = 1/\rho$, for which the continuity equation becomes:

$$\nabla(\kappa_b \nabla V_b) = 0 \tag{A7}$$

where V_b describes the potential field in the homogenized resistivity field, subject to the same boundary conditions as in (A6).

Appendix B: Conditional Mean Sampling

For an arbitrary covariance matrix, generating random samples from a joint normal distribution with given values of some linear combinations is not difficult, because all linear combinations of jointly normal random variables are jointly normal, which means that the conditional distributions are also jointly normal. The procedure is to subtract the regression of the various variables on the constraints; i.e., assuming the n random variables $r_1, \cdots, r_i, \cdots, r_n$ are generated from different Gaussian pdf $f''_1(r;\ m''_1,\ \sigma''_1), \cdots, f''_n(r;\ m''_n,\ \sigma''_n)$, respectively, all r_i have to average to the resistivity survey ρ. For an arithmetic average, the difference between ρ and the sampled $\bar{r} = \Sigma_l\, r_l/n$ is then subtracted from each r_l as follows:

$$r''_l = r_l - (\bar{r} - \rho) \tag{B1}$$

where r'' is the posterior resistivity. For a geometric mean the procedure remains valid, but the resistivity should be replaced by its logarithm: ln (r).

To take into account the variability for each pdf, one should weight the corrected resistivity value with respect to their relative inertia, as follows:

$$r''_l = r_l - n\sigma_l^2(\bar{r} - \rho)/\sum_m \sigma_m^2 \quad \text{(B2)}$$

Since corrections are deterministic, statistics of each distribution remain the same.

Acknowledgments. Funding for this study was provided by the Department of Energy, Environmental Management Science Program grant DE-FG07-96ER14726. Additional support was made available by NSF through grant EAR 9628306. The authors wish to thank G. Mavko, and T. Mukerji from Stanford University, Geophysics Department; R. Bainer and R. Blake from Lawrence Livermore National Laboratories, Environmental Restoration Division; D. G. Hill from Weiss Associates; and J. Rector, H. F. Morrison, and R. Hatch from University of California at Berkeley, Engineering Geosciences Department.

References

Abramovich, B., and P. Indelman, Effective permittivity of log-normal isotropic random media, *J. Phys. A Math. Gen*., *28*(3), 693–700, 1995.

Ang, A. H.-S., and W. Tang, *Probability Concepts in Engineering Planning and Design*, John Wiley, New York, 1975.

Beard, L. P., G. W. Hohmann, and A. C. Tripp, Fast resistivity/IP inversion using a low-constant approximation, *Geophysics*, *61*(1), 169–179, 1996.

Bilal, A. M., and M. M. Gupta, *Uncertainty Analysis in Engineering and Sciences: Fuzzy Logic, Statistics and Neural Network Approach*, Kluwer Acad., Norwell, Mass., 1997.

Blake, R., M. P. Maley, and C. M. Noyes, Characterization of VOC transport in heterogeneous sediments at Lawrence Livermore National Laboratory and its impact on remediation decisions, paper presented at 1995 Annual Meeting, Assoc. of Eng. Geol., Sacramento, Calif., 1995.

Cassiani, G., G. Bohm, A. Vesnaver, and R. Nicolich, A geostatistical framework for incorporating seismic tomography auxiliary data into hydraulic conductivity, *J. Hydrol*., *206*(1–2), 58–74, 1998.

Chew, W. C., *Waves and fields in inhomogeneous media*, *Ser. Electromagn. Waves Theory*, IEEE Press, Piscataway, N. J., 1995.

Copty, N., and Y. Rubin, A stochastic approach to the characterization of lithofacies from surface seismic and well data, *Water Resour. Res*., *31*(7), 1673–1686, 1995.

Dagan, G., *Flow and Transport in Porous Formations*, Springer-Verlag, New York, 1989.

Daily, W., A. Ramirez, D. LaBrecque, and J. Nitao, Electrical resistivity tomography of vadose water movement, *Water Resour. Res*., *28*(5), 1429–1442, 1992.

Deutsch, C. V., and A. Journel, *GSLIB: Geostatistical Software Library and User's Guide Version 2.0*, 2nd ed., Oxford Univ. Press, New York, 1998.

Doveton, J. H., *Log Analysis of Subsurface Geology: Concepts and Computer Methods*, John Wiley, New York, 1986.

Doyen, P. M., Porosity from seismic data: A geostatistical approach, *Geophysics*, *53*(10), 1263–1276, 1988.

Hill, D. G., Geophysical well log calibration and quality control, in *Borehole Geophysics for Mining and Geotechnical Applications*, *Publ. 85-27*, pp. 379–392, Geol. Surv. of Can., 1986.

Hubbard, S. S., Y. Rubin, and E. Majer, Ground-penetrating-radar-assisted saturation and permeability estimation in bimodal systems, *Water Resour. Res*., *33*(5), 971–990, 1997.

Hubbard, S. S., Y. Rubin, and E. Majer, Spatial correlation structure estimation using geophysical and hydrogeological data, *Water Resour. Res*., *35*(6), 1809–1825, 1999.

Hyndman, D. W., J. M. Harris, and S. M. Gorelick, Coupled seismic and tracer test inversion for aquifer property characterization, *Water Resour. Res*., *30*(7), 1965–1977, 1994.

Keys, W. S., *Borehole Geophysics Applied to Ground-Water Investigations*, Natl. Water Well Assoc., Dublin, Ohio, 1997.

Lucet, N., and G. Mavko, Images of rock properties estimated from a crosswell seismic velocity tomogram, (abstract), in *1991 Technical Program and Abstracts of Papers*, vol. 53, pp. 520–521, Eur. Assoc. of Explor. Geophys., Florence, Italy, 1991.

Mavko, G., T. Mukerji, and J. Dvorkin, *The Rock Physics Handbook: Tools for Seismic Analysis in Porous Media*, Cambridge Univ. Press, New York, 1998.

Noyes, C. D., Hydrostratigraphic analysis of the pilot remediation test area, Lawrence Livermore National Laboratory, Livermore, California, MS thesis, 163 pp., Univ. of Calif., Davis, 1991.

Rubin, Y., *Flow and transport in bimodal heterogeneous formations*, *Water Resour. Res*., *31*(10), 2461–2468, 1995.

Rubin, Y., and A. Bellin, Conditional simulation of geologic media with evolving scales of heterogeneity, in *Scale Dependence and Scale Invariance in Hydrology*, edited by G. Sposito, pp. 398–420, Cambridge Univ. Press, New York, 1998.

Rubin, Y., G. Mavko, and J. Harris, Mapping permeability in heterogeneous aquifers using hydrologic and seismic data, *Water Resour. Res*., *28*(7), 1809–1816, 1992.

Serra, O., Fundamentals of well-log interpretation, *Dev. Pet. Sci*., *15*A-B, 1984.

Sheets, K. R., and J. M. H. Hendricks, Noninvasive soil water content measurement using electromagnetic induction, *Water Resour. Res*., *31*(10), 2401–2409, 1995.

Telford, W. M., L. P. Geldart, and R. E. Sheriff, *Applied Geophysics*, 2nd ed., Cambridge Univ. Press, New York, 1990.

Woodbury, A. D., and T. J. Ulrych, Minimum relative entropy: Forward probabilistic modeling, *Water Resour. Res*., *29*(8), 2847–2860, 1993.

J. Chen, S. Ezzedine, and Y. Rubin, Department of Civil and Environmental Engineering, 440 Davis Hall, University of California, Berkeley, CA 94720-1710. (rubin@ce.berkeley.edu)

(Received February 17, 1999; revised April 16, 1999;
accepted April 19, 1999.)